Investigating the role of cloud-radiation interactions in subseasonal tropical disturbances

James J. Benedict^{1,2}, Brian Medeiros³, Amy C. Clement¹, Jerry G. Olson³

- ¹Rosenstiel School of Marine and Atmospheric Science, University of Miami, Miami, Florida, USA.
- ²Visiting Scientist, Climate and Global Dynamics Laboratory, National Center for Atmospheric Research,
- Boulder, Colorado, USA.
- ³Climate and Global Dynamics Laboratory, National Center for Atmospheric Research, Boulder,
- Colorado, USA.

Key Points:

2

11

- Disabling cloud-radiation interactions in CESM2 weakens the MJO but strengthens Kelvin waves
- MJO survives via sustained advection and surface fluxes despite weak cloud effects and increased gross moist stability
 - Kelvin waves strengthen due to reduced convective inhibition and reduced radiative damping of temperature variance

Corresponding author: James J. Benedict, jjb278@gmail.com

Abstract

16

Cloud locking, a method that prescribes cloud properties for radiative tendency calcu-17 lations, is traditionally used to explore climate feedbacks but here is applied novelly to investigate cloud-radiation interaction (CRI) impacts on subseasonal tropical variabil-19 ity. The approach minimizes mean state differences between control (CRI active) and experimental simulations (CRI disabled) of the Community Earth System Model. Dis-21 abling CRI weakens amplitudes of the Madden-Julian oscillation (MJO) by 10–35% and 22 equatorial Rossby waves by 10-30% yet strengthens Kelvin waves by 10-40%. MJO weak-23 ening results from suppressed radiation-convection positive feedbacks and increased gross 24 moist stability. Kelvin waves strengthen from reduced convective inhibition and reduced 25 radiative damping on temperature variance. The results are compared to a recently pro-26 posed theory that describes a continuum of tropical disturbances. MJO survival, when 27 its primary maintenance mechanism (CRI) is eliminated, stresses the importance of ad-28 vection and surface flux processes.

30 Plain language summary

Tropical cloud systems exist on many scales, from squall lines to continent-sized cloud 31 systems. Solar and thermal radiation interact with these cloudy "disturbances" in ways 32 that can favor further development of the disturbance. The exact nature of these interactions along with associated changes to other disturbance properties such as winds, temper-34 ature, and surface evaporation—are inadequately understood and therefore cause inaccuracies in weather and climate prediction models. We investigate the impact of cloud-36 radiation interactions by preventing clouds from interacting with radiative heating in our 37 model. In response, certain types of tropical cloud disturbance become weaker while oth-38 ers strengthen. These results highlight the distinct roles of cloud feedbacks for different 39 tropical phenomena and demonstrate how a poor representation of cloud processes might 40 degrade the accuracy of weather and climate models. 41

1 Introduction

42

43

45

47

49

50

51

52

53

54

59

60

61

63

65

67

69

70

71

72

Clouds—by serving as the site of latent heat release, modulating radiative fluxes, and redistributing heat, momentum, and moisture—have a profound impact on Earth's climate. Cloud distribution, height, and thickness determine the cloud radiative effect (CRE), defined as the difference between actual and clear-sky top-of-atmosphere (TOA) net radiative flux. CRE metrics may alternatively use surface rather than TOA fluxes, or include the entire atmospheric column ["ACRE", Fermepin and Bony, 2014] to more directly link clouds and circulation. For simplicity, we label the totality of these effects "cloud-radiation interaction" (CRI). It has long been established in observational records that CRI strongly influences Earth's energy budget [Hartmann and Short, 1980]. Particular attention has been paid to the tropics, where annual mean insolation is largest and cloud processes are both highly variable and difficult to represent in global climate models [GCMs; e.g., Randall et al., 2003]. GCM studies of the tropics demonstrate how CRI influences the distribution of precipitation [Neelin and Held, 1987; Slingo and Slingo, 1988; Harrop and Hartmann, 2016], large-scale circulations [Raymond, 2000], and climate response to global warming [Bretherton, 2015]. Myriad studies also highlight CRI impacts on interannual and inter-decadal variability across the Atlantic [Bellomo et al., 2015, 2016] and Pacific basins [Bellomo et al., 2014; Rädel et al., 2016; Middlemas et al., 2019].

CRI modulation of subseasonal tropical variability is also an active area of research. Central to this is the Madden-Julian oscillation [MJO; Madden and Julian, 1971], the dominant mode of tropical variability on intraseasonal scales (20-100 day periods). The MJO has far-reaching impacts across wide space-time scales [Zhang, 2005]. MJO disturbances—and, more broadly, the realistic amplitude and distribution of tropical subseasonal variability—are poorly simulated in many GCMs [Hung et al., 2013] due to inadequate understanding of interactions among convection, radiation, and the large-scale circulation.

Insight into large-scale tropical convection-circulation coupling can be gleaned from analysis of the moist static energy budget [MSE; e.g., Maloney, 2009] and gross moist stability [GMS; Neelin and Held, 1987; Raymond et al., 2009]. Tropical precipitation is a strongly varying function of vertically integrated (hereafter, "column") water vapor amount [Bretherton et al., 2004], which equates to column MSE under weak temperature gradient conditions that characterize the tropics [Sobel et al., 2001]. Many studies

suggest that MJO-like disturbances called "moisture modes" [Sobel et al., 2001; Fuchs and Raymond, 2005] are destabilized when the net effect of convection and related diabatic processes amplify column MSE anomalies. GMS encapsulates these complex process interactions by quantifying the net column MSE export per unit convective activity. Moisture mode disturbances are more likely to develop if GMS is negative or weakly positive [Haertel et al., 2008; Raymond and Fuchs, 2009; Benedict et al., 2014]. GMS can be reduced by diabatic processes such as surface fluxes or cloud radiative feedbacks [Sobel and Maloney, 2013], the subject of this study.

Numerous idealized modeling studies propose theories that describe how CRI influences tropical waves [Hu and Randall, 1994; Raymond, 2001; Bretherton and Sobel, 2002; Fuchs and Raymond, 2002; Sobel and Gildor, 2003; Bony and Emanuel, 2005; Sugiyama, 2009; Andersen and Kuang, 2012; Sobel and Maloney, 2013; Arnold and Randall, 2015; Adames and Kim, 2016; Khairoutdinov and Emanuel, 2018; Emanuel, 2019]. These theories state that, in the disturbance's convectively active phase, increased cloudiness and water vapor reduce thermal emission to space. The reduced OLR reinforces preexisting convective (latent) heating, thus acting as a so-called "greenhouse enhancement factor" [Bretherton and Sobel, 2002; Kim et al., 2015]. Observational evidence supports this proposed feedback mechanism [Lin and Mapes, 2004]. Other idealized tropical models suggest that suppressed OLR also drives positive advection feedbacks that favor moisture mode amplification [Raymond, 2001].

Comprehensive GCMs have also been used to investigate CRI impacts on tropical subseasonal variability. Most studies report that disabling CRI weakens MJOs [Kim et al., 2011a; Ma and Kuang, 2016], although the degree of MJO suppression is model-dependent. Other studies, however, indicate stronger intraseasonal variability with CRI removed [Lee et al., 2001], or that CRI has little impact on MJO-like disturbances [Grabowski and Moncrieff, 2001; Grabowski, 2003; Lin et al., 2007].

Several modeling studies use methodologies that complicate interpretation of the results. One key limitation is the use of prescribed zonally or globally uniform SSTs, which can produce time mean circulation and moisture distributions unlike those observed in the equatorial Indo-Pacific and can generate disturbances whose driving mechanisms differ from those observed [Khairoutdinov and Emanuel, 2018]. Another limitation arises in how CRI is disabled. Some studies impose space-time averaged radiative heating from

a control simulation on the experimental run [Shi et al., 2018]; others apply nudging and time-invariant forcing [Ma and Kuang, 2016]. Although these approaches reduce mean state differences, they also represent a more intrusive modification of the atmospheric state. Yet other studies simply set cloud cover to zero when computing radiative heating [Crueger and Stevens, 2015], which alters the mean state and makes isolating CRI effects on tropical variability more challenging.

In this study, a series of GCM experiments is performed to better understand how CRI impacts tropical subseasonal variability. We implement the "cloud locking" technique whereby the cloud properties that the radiative transfer scheme receives is taken from a separate simulation [e.g., Langen et al., 2012; Mauritsen et al., 2013]. While previous studies use cloud locking to investigate climate feedbacks [e.g., Ceppi and Hartmann, 2016], interannual variability [Rädel et al., 2016; Middlemas et al., 2019], and extratropical storms [Schäfer and Voigt, 2018; Grise et al., 2019], application of this approach to tropical subseasonal variability is novel. Cloud locking decouples CRI from the circulation while maintaining similar mean states between control and experimental simulations. Isolating the role of CRI in this way provides greater clarity into its impact on simulated variability, including a refined assessment of model biases associated with subseasonal tropical disturbances. We find that CRI significantly affects all wave types, indicating that CRI-related model biases can impact the full spectrum of tropical variability beyond just the mean state.

2 Methods

We investigate CRI's impact on tropical subseasonal variability in Community Earth System Model version 2.0.1 ("CESM2") simulations run on NCAR's Cheyenne supercomputer [Computational and Information Systems Laboratory, 2017]. Atmospheric processes are simulated by the Community Atmosphere Model version 6.0 [CAM6; Bogenschutz et al., 2018], which uses the Cloud Layers Unified by Binormals (CLUBB) scheme as an update to boundary layer, turbulence, shallow convection, and cloud macrophysics parameterizations of previous CAM versions. Further details of CAM6 and other CESM2 components are found at: http://www.cesm.ucar.edu/models/cesm2/.

Four CESM2 simulations are conducted. All span 25 yr (excluding a discarded 3-yr spinup period) and use prescribed pre-industrial atmospheric composition. The first

138

139

140

141

142

143

144

145

146

147

148

149

150

151

152

153

154

155

156

157

158

159

160

161

162

163

164

165

166

167

168

simulation (CTL) uses realistic CRI with prognostic atmosphere, land, ocean, and sea ice models. CTL is initialized from Year 263 of an existing fully coupled pre-industrial control simulation with an equilibrated climate. The second run (CLOCK) is identical to CTL except that cloud properties used to compute radiative heating are prescribed ("locked") rather than being sourced from CLOCK's current predicted state. A listing of prescribed cloud properties Σ_{cld} appears in Middlemas et al. [2019]. CLOCK's Σ_{cld} are instantaneous, 2-hourly snapshots sourced from Years 20-22 of CTL ("data pool"), a 3-yr span with near-neutral ENSO conditions. Similar to $R\ddot{a}del$ et al. [2016], Σ_{cld} from a randomly selected year within the CTL data pool are applied to each CLOCK hourly radiation call (identical 2-hourly Σ_{cld} are applied on consecutive hourly calls). The calendar day and time of day of Σ_{cld} match those of CLOCK to maintain proper seasonal and diurnal variability. Our approach differs slightly from Middlemas et al. [2019], who use sequential and annually repeating Σ_{cld} from one year of their control run. The cloudlocking method precisely disables CRI without directly altering the atmospheric state, and ensures similar CTL-CLOCK climatologies. Importantly, CRI in CLOCK has zero temporal autocorrelation (no "memory") and cloud-radiative processes are fully decoupled from the predicted dynamical state.

To examine potential sensitivities to air-sea coupling, we conduct two atmosphereonly versions of CTL and CLOCK that use fixed SST and sea ice: FCTL and FLOCK. FCTL uses time-evolving SSTs and sea ice from CTL as oceanic lower boundary conditions. Like CTL, FCTL implements realistic CRI. A fourth run—FLOCK—is identical to FCTL except that cloud locking is imposed using Σ_{cld} from Years 20-22 of CTL, as was done in CLOCK.

Because the mean state can strongly impact disturbance behavior [Kim et al., 2011b], minimizing mean state differences between control and experimental simulations is essential to isolate CRI impacts on tropical variability. Only modest differences in time-mean precipitation (Fig. S1) and 850 hPa zonal wind (Fig. S2) exist between FCTL and FLOCK. Larger mean state differences exist between CTL and CLOCK (Fig. S3) and potentially arise from (a) nonlinearities of the modified CRI on the surface energy budget and/or (b) an insufficiently large data pool from which Σ_{cld} are sourced. As shown in Sec. 3, cloud locking impacts on tropical subseasonal variability are very similar between CLOCK and FLOCK, indicating that the larger CTL-CLOCK mean state dif-

ferences have little bearing on our results. For the remainder of this paper, we focus on the FCTL–FLOCK simulation pair.

3 Results: Impacts of locking

169

170

171

172

173

174

175

176

177

178

179

180

181

182

183

184

185

186

187

188

190

192

193

194

195

196

197

198

199

With CRI eliminated in FLOCK, the spectrum of subseasonal variability is strongly altered. Figure 1 presents non-normalized zonal wavenumber-frequency power spectra of precipitation, following Wheeler and Kiladis [1999]. Some power enhancement in FCTL (Figs. 1a,d) is apparent for the MJO and equatorial Rossby (ER), Kelvin, and mixed Rossby-gravity (MRG) waves. Compared to Tropical Rainfall Measurement Mission [Huffman et al., 2007 precipitation estimates (not shown), FCTL underestimates spectral power of high frequency Kelvin waves (periods < 8 days) by $\sim 30-60\%$ and the MJO by $\sim 20-$ 50%, a deficiency common to many CMIP5-class GCMs [Hung et al., 2013]. Additional analysis (Fig. S8) confirms the lack of a robust MJO in CESM2, especially for FCTL; this must be considered when interpreting the results below. Non-normalized power for FLOCK (Figs. 1b,e) suggests enhanced Kelvin wave activity with weakened ER wave and MJO variability. Plotting the (FLOCK-FCTL)/FCTL difference (Figs. 1c,f) clarifies these changes. Importantly, the spectral changes are not simply a function of frequency but are instead sensitive to wave type: gravity-type waves (interia-gravity, Kelvin, and a portion of MRG waves) are favored in FLOCK while ER waves and the MJO are weakened. In FLOCK, Kelvin wave precipitation spectral power increases by 10–40%, ER wave variability decreases by 20–30% and MJO variability declines by 10–25% compared to FCTL. Corresponding spectra for CTL-CLOCK (Fig. S4) are similar to the FCTL-FLOCK results (Fig. 1), indicating that cloud locking effects far outweigh airsea coupling processes or mean state differences (Fig. S3). Changes to corresponding 850 hPa zonal wind spectra (Fig. S5) are consistent with the precipitation results. Variance maps of wave-filtered precipitation (not shown) indicate that cloud locking preferentially suppresses both MJO and ER waves in regions where these respective wave types are climatologically most active.

What causes the tropical variability change when CRI is disabled? Several lines of argument—those based on the vertically integrated MSE budget, analysis of key tropical precipitation controls, and a shallow water theoretical framework—are invoked to better characterize and plausibly explain shifts in tropical variability. The following anal-

ysis focuses on the MJO and Kelvin waves as they encapsulate the changes seen in Fig. 1.

3.1 Understanding MJO weakening

200

201

202

203

204

206

207

208

209

210

211

213

215

216

217

218

219

220

221

222

224

225

226

227

228

229

230

231

The moisture mode hypothesis states that MJO-like disturbances are dynamically destabilized when advective and diabatic processes sustain a net import of column MSE. It is therefore useful to examine column MSE budget terms to elucidate why the MJO weakens in FLOCK. Lag composited column MSE budget components for FCTL and FLOCK intraseasonal disturbances in the Indian Ocean (IO) and west Pacific (WP) sectors are displayed in Figure 2 along with corresponding precipitation anomalies upon which the composites are based (bottom row). All data are 30–100-day filtered to isolate MJO variability (see caption and Text S1 for method details). In FCTL, the initial increase in column h is driven primarily by advection terms $\langle -\mathbf{v}\cdot\nabla h\rangle$ and $\langle -\omega\partial_n h\rangle$, which lead h tendency $\langle \partial_t h \rangle$ by less than 1/4 cycle. Longwave heating $\langle LW \rangle$ lags $\langle \partial_t h \rangle$ by 1/4 cycle and is nearly out of phase with h advection, while surface heat fluxes oppose $\langle \partial_t h \rangle$. The strong positive correlation between (LW) and precipitation and its phase quadrature with $\langle \partial_t h \rangle$ indicate that $\langle LW \rangle$ primarily supports MJO amplification rather than MJO propagation, as shown previously [e.g., Andersen and Kuang, 2012]. Interpretation of the terms, particularly those with smaller amplitude, is clouded by the non-negligible budget residual.

Disabling CRI in FLOCK (middle row, Fig. 2) virtually eliminates contributions from $\langle LW \rangle$, yet MJO precipitation amplitude decreases by $\sim 20\%$ (WP) to $\sim 35\%$ (IO) compared to FCTL (Fig. 2c,f), with "amplitude" x defined as $(|\max(x)| - |\min(x)|)/2$ and cloud locking-related changes defined as (FLOCK–FCTL)/FCTL. The 20–35% precipitation amplitude suppression is consistent with the reduction of MJO spectral power (Figs. 1c,f). In FLOCK, surface fluxes become more in phase with precipitation, signaling their increased role for MJO amplification, while the phasing of h advection remains largely unchanged from FCTL. Decreased amplitudes of h advection (-60% IO, -34% WP) and $\langle \partial_t h \rangle$ (-44% IO, -20% WP) and the near elimination of $\langle LW \rangle$ (-90% IO and WP) are noted. Remnant $\langle LW \rangle$ effects likely arise from a positive covariance between anomalous water vapor, which is not a "locked" variable, and radiation. Surface heat flux amplitude responses are basin-dependent: -23% for IO events, +65% for WP events. Thus, interpretation of the role of surface heat fluxes requires caution, given the non-

negligible budget residual and geographic sensitivity. The somewhat surprising result that the MJO does not vanish when CRI is disabled is also reported in previous studies [Arnold and Randall, 2015; Ma and Kuang, 2016; Khairoutdinov and Emanuel, 2018]. Our results provide additional evidence of the critical role that MSE advection plays in MJO propagation, which is robust for composite MJO events across longitude and is consistent with several earlier works [e.g., Benedict and Randall, 2007; Pritchard and Bretherton, 2014; Adames and Kim, 2016].

3.2 MJO and Kelvin wave responses: Inferences from hypothesized precipitation controls

Fluctuations of column moisture, surface heat fluxes, and convective inhibition (CIN)—the energy needed to lift an air parcel from the near-surface layer to the level at which it becomes positively buoyant—strongly regulate observed large-scale tropical disturbances [Firestone and Albrecht, 1986; Raymond, 1995; Bretherton et al., 2004]. Leveraging these observed sensitivities, toy atmosphere models can reproduce key behaviors of disturbances resembling convectively coupled Kelvin waves and the MJO [e.g., Mapes, 2000; Raymond and Fuchs, 2007]. Of particular relevance to this study are the results of Raymond and Fuchs [2007], who found distinct differences in the three factors as they relate to moisture modes and atmospheric Kelvin waves. In their study, moisture mode precipitation is driven primarily by column moisture variations and secondarily by surface moist entropy fluxes; fluctuations in CIN play virtually no role. In contrast, Kelvin wave precipitation is dominated by CIN variations—especially CIN reductions due to wave-induced cooling immediately above the boundary layer—while the other terms are less important [Raymond and Fuchs, 2007].

Table 1 presents zero-lag regression coefficients of fields hypothesized to strongly control MJO and Kelvin wave precipitation based on observations and idealized model results [Raymond and Fuchs, 2007]. Results are scaled by precipitation intensity; see Table 1 caption and Text S6 for further details. For the MJO, cloud locking drives a reduction of anomalous column moisture, little change in deep convective inhibition (DCIN), and increased surface latent heat fluxes, though the latter has a strong geographical sensitivity as noted in Sec. 3.1. However, enhanced Kelvin waves in FLOCK arise primarily from significantly reduced DCIN resulting from decreased $\overline{h^*}_{\rm t}$ (cooling immediately above the boundary layer top). As will be discussed in Sec. 4 (see Fig. S6), this low-level

cooling is coupled with upper-tropospheric warming, which aligns with the stratiform instability mechanism introduced by Mapes [2000] to describe Kelvin wave destabilization. Our results are also strikingly similar to those produced by the toy model of Ray-mond and Fuchs [2007] and underscore the importance of CIN in regulating moist Kelvin waves.

3.3 Shallow water scaling

The shift in tropical wave activity when CRI is disabled in CESM2 (Figs. 1c and 1f) also supports the recent work of Adames et al. [2019]. In their paper, a shallow water scaling analysis is used to identify processes that determine preferred development of disturbances across a continuum that spans moisture modes (e.g., the MJO) to gravity waves (e.g., Kelvin waves). The type of disturbance that develops is dependent on a non-dimensional parameter N^*_{mode} : gravity waves are favored when $|N^*_{mode}| \gg 1$ and moisture modes are favored when $|N^*_{mode}| \ll 1$. Although the scaling framework presented by Adames et al. [2019] is highly idealized, it's relevance to our results is pertinent. Insight is gained by examining how CRI affects N^*_{mode} and thus the preferred growth of either moisture modes or gravity waves. We can leverage the fact that $N^*_{mode} \propto \widetilde{M}_{eff}$, where \widetilde{M}_{eff} is the effective GMS that includes diabatic processes. From Eq. 14 of Hannah and Maloney [2014], a suitable expression of effective GMS is

$$\widetilde{M}_{eff} = \frac{\langle -\omega \partial_p h \rangle + \langle Q_R \rangle + \text{LH} + \text{SH}}{\langle -\omega \partial_p s \rangle}, \tag{1}$$

where $-\omega \partial_p h$ and $-\omega \partial_p s$ represent vertical advection of MSE and dry static energy (respectively), Q_R is the net radiative heating rate, LH and SH are surface latent and sensible heat fluxes (respectively), and angled brackets represent a mass-weighted integral from the surface to 100 hPa.

We find that \widetilde{M}_{eff} is higher in FLOCK than in FCTL on both seasonal and subseasonal scales (Fig. 3). Following Hannah and Maloney [2014], an aggregate form of \widetilde{M}_{eff} is assessed by averaging the numerator of (1) based on bins of $\langle -\omega \partial_p s \rangle$ using daily data from across the Indo-Pacific Warm Pool (see Text S4 for method details). For nearly all bins in which the quotient of (1) is well behaved (bin centers corresponding to $|\langle -\omega \partial_p s \rangle| > 150 \,\mathrm{W\,m^{-2}}$), Fig. 3a indicates that time-mean \widetilde{M}_{eff} is significantly higher in FLOCK than

in FCTL. Figure 3b reveals that anomalous \widetilde{M}_{eff} is also significantly higher in FLOCK over a composite MJO lifecycle (see Text S5).

What drives the \widetilde{M}_{eff} changes of Fig. 3? In (1), CRI influences \widetilde{M}_{eff} directly through $\langle Q_R \rangle$ but also can potentially impact \widetilde{M}_{eff} indirectly through changes in the other terms. A separate analysis (Fig. S7) of the various terms that contribute to \widetilde{M}_{eff} signals that FCTL-FLOCK differences in both the normalized (Fig. 3a) and non-normalized (Fig. S7c) forms of \widetilde{M}_{eff} are driven almost exclusively by changes in $\langle Q_R \rangle$ while contributions from the other terms of (1) are similar between FCTL and FLOCK. We have therefore isolated the mechanism by which our imposed changes in CRI cause shifts in tropical disturbance regimes: as cloud locking suppresses cloud-radiation feedbacks, \widetilde{M}_{eff} increases which contributes to an increase in N^*_{mode} and thus preferentially favors gravity wave development (e.g., Kelvin waves) over moisture mode growth (e.g., MJO).

4 Summary and discussion

Cloud locking, a method in which cloud-radiation interactions (CRI) are disabled in a GCM simulation, is used to investigate the role of CRI on subseasonal tropical atmospheric variability. This approach, as applied to subseasonal tropical variability, is novel and precisely isolates CRI impacts on tropical disturbances while minimizing mean state differences (Figs. S1 and S2). We focus on two prescribed-SST CESM2 simulations, one with natural CRI (FCTL) and one with CRI disabled (FLOCK). Cloud locking dramatically alters the distribution of subseasonal variability in spectral space (Fig. 1), damping so-called "moisture modes" (i.e., MJO and equatorial Rossby waves) while enhancing gravity-type waves (e.g., atmospheric Kelvin waves, mixed Rossby-gravity waves, and interia-gravity waves). A separate investigation of CESM2 simulations with interactive SSTs suggests that our results are largely insensitive to air-sea coupling strategy and mean state differences (e.g., Fig. S3).

The MJO and Kelvin waves, selected as representative moisture mode and gravity wave disturbances (respectively), are examined to identify key mechanisms that plausibly explain the subseasonal variability changes between FCTL and FLOCK. Although column longwave heating is the dominant contributor to MJO amplification in FCTL, disabling CRI weakens the MJO by $\sim 20-35\%$ but does not eliminate it (Fig. 2). This somewhat surprising result is also reported in aquaplanet studies using prescribed "global"

Warm Pool" SSTs [Arnold and Randall, 2015; Khairoutdinov and Emanuel, 2018] or Earth-like equator-pole SST gradients [Andersen and Kuang, 2012; Shi et al., 2018]; however, the climatological low-level tropical easterlies simulated in these models could support MJO mechanisms unlike those observed in the Warm Pool region (60°E–170°E), which exhibits low-level westerlies during boreal winter. MJO suppression in CESM2 is not as strong as in other CGM studies with CRI disabled [Kim et al., 2011a; Ma and Kuang, 2016]. MJO "survival" in FLOCK results from sustained (but damped) contributions from MSE advection that drives MJO propagation, and from surface heat fluxes that become more in phase with MJO precipitation (Fig. 2) thus working to maintain or weakly amplify the disturbance, though we note that the surface heat flux response is strongly geographically dependent in our simulations.

Convectively coupled Kelvin waves amplify when CRI is disabled in our CESM2 simulations due to reduced convective inhibition (CIN) driven by wave-induced cooling in the lower free troposphere (Table 1). This behavior is consistent with the stratiform instability mechanism of *Mapes* [2000] and related toy model simulations of the tropical atmosphere [e.g., *Raymond and Fuchs*, 2007]. Separate examinations (Fig. S6) reveal a negative covariance between radiation and temperature anomalies for FCTL Kelvin waves, but this damping is muted in FLOCK leading to strengthened Kelvin waves driven by greater eddy available potential energy (EAPE) generation that acts as a source of Kelvin wave instability (the opposite behavior is generally noted for the MJO).

The shallow water scaling analysis of Adames et al. [2019], which characterizes tropical disturbances as a continuum spanning moisture modes and gravity waves, provides another theoretical framework to compare our model results. FLOCK exhibits increased effective gross moist stability (GMS) both on time mean and subseasonal scales (Fig. 3) that is driven by reduced sensitivity of column longwave heating to convective variability (Fig. S7). The increased GMS in FLOCK increases parameter N_{mode}^* which, following Adames et al. [2019], favors gravity waves over moisture modes. This conclusion requires that other variables upon which N_{mode}^* depends—including convective moisture adjustment time scale τ_c and gravity wave adjustment time scale τ_g —remain reasonably unchanged with cloud locking. This assumption appears to be valid: τ_g is sensitive to static stability, which differs by less than 10% in the Indo-Pacific time mean between FCTL and FLOCK (not shown), and similarly modest differences are noted for τ_c (Fig. S9). Our results may be consistent with a continuum disturbance perspective: by eliminat-

ing one diabatic feedback, we suppress the MJO and simultaneously amplify Kelvin waves, particularly lower-frequency Kelvin waves (Fig. 1). MJO-like disturbances have greater resemblance to Kelvin waves when they decouple from deep convection [e.g., *Matthews*, 2000]; we hypothesize that cloud locking represents a partial decoupling of diabatic heating from the circulation, so it is not unexpected that our results are consistent with this behavior. Further exploratory research is needed to address potential limitations of the continuum theory as well as applicability of our results to it, however.

Cloud locking highlights key processes that impact subseasonal tropical disturbances. It also represents an extreme form of model bias and can be leveraged to advance model development. GCM CRI biases exist to varying degrees, but their manifestation may not be readily apparent due to natural variability or other bias sources. Cloud locking artificially amplifies CRI biases to clearly expose how they impact simulations. Our results demonstrate that misrepresenting CRI in GCMs can impact not only the mean state but also subseasonal tropical variability, which strongly influences weather and climate globally [Roundy, 2012, and references therein].

We have shown how CRI mediates both the large-scale circulation and moist convection on subseasonal time scales, but several questions remain. Given the non-negligible MSE budget residual and geographic sensitivities, what are the detailed roles of CRI and surface fluxes for tropical disturbance maintenance and propagation? Why does elimination of CRI, the dominant source of diabatic heating for MJO amplification, not fully suppress the MJO? Does the similar number of identified MJO events in FCTL and FLOCK suggest that CRI is not critical to MJO initiation? To what extent is the MJO a manifestation of a Kelvin wave heavily modified by diabatic processes? These probing questions warrant further investigation in future studies.

Acknowledgments

We thank two anonymous reviewers for their helpful feedback, and Á. Adames, K. Grise,
E. Maloney, E. Middlemas, D. Randall, and B. Wolding for stimulating conversations.

CESM2 outputs available at https://zenodo.org keyword search "CESMcloudlocking".

National Science Foundation (NSF) award AGS-1650209 funded JB and AC. This material is based upon work supported by NCAR, a major facility sponsored by the NSF under Cooperative Agreement No. 1852977. The CESM project is supported primarily by the NSF. Partial support also comes from the Regional and Global Model Anal-

- ysis (RGMA) component of the Earth and Environmental System Modeling Program
- of the U.S. Department of Energy's Office of Biological & Environmental Research (BER)
- via NSF IA 1844590. Computing and data storage resources, including the Cheyenne su-
- percomputer (doi:10.5065/D6RX99HX), were provided by CISL at NCAR.

References

392

- Adames, Á. F., and D. Kim (2016), The MJO as a dispersive, convectively cou-
- pled moisture wave: Theory and observations, J. Atmos. Sci., 73(3), 913–941,
- doi:10.1175/jas-d-15-0170.1.
- Adames, Á. F., D. Kim, S. K. Clark, Y. Ming, and K. Inoue (2019), Scale analysis of
- moist thermodynamics in a simple model and the relationship between moisture
- modes and gravity waves, J. Atmos. Sci., doi:10.1175/jas-d-19-0121.1.
- Andersen, J. A., and Z. Kuang (2012), Moist static energy budget of MJO-like
- disturbances in the atmosphere of a zonally symmetric aquaplanet, J. Climate,
- 25(8), 2782-2804, doi:10.1175/jcli-d-11-00168.1.
- Arnold, N. P., and D. A. Randall (2015), Global-scale convective aggregation: Im-
- plications for the Madden-Julian Oscillation, J. Adv. Model. Earth Syst., 7(4),
- 404 1499–1518, doi:10.1002/2015ms000498.
- Bellomo, K., A. Clement, T. Mauritsen, G. Rädel, and B. Stevens (2014), Simulating
- the role of subtropical stratocumulus clouds in driving pacific climate variability,
- J. Climate, 27(13), 5119–5131, doi:10.1175/jcli-d-13-00548.1.
- Bellomo, K., A. C. Clement, T. Mauritsen, G. Rädel, and B. Stevens (2015), The
- influence of cloud feedbacks on equatorial atlantic variability, J. Climate, 28(7),
- 410 2725–2744, doi:10.1175/jcli-d-14-00495.1.
- Bellomo, K., A. C. Clement, L. N. Murphy, L. M. Polvani, and M. A. Cane (2016),
- New observational evidence for a positive cloud feedback that amplifies the
- atlantic multidecadal oscillation, Geophys. Res. Lett., 43(18), 9852–9859, doi:
- 414 10.1002/2016gl069961.
- Benedict, J. J., and D. A. Randall (2007), Observed characteristics of the MJO rela-
- tive to maximum rainfall, J. Atmos. Sci., 64(7), 2332–2354, doi:10.1175/jas3968.1.
- Benedict, J. J., E. D. Maloney, A. H. Sobel, and D. M. W. Frierson (2014), Gross
- moist stability and MJO simulation skill in three full-physics GCMs, J. Atmos.
- Sci., 71(9), 3327–3349, doi:10.1175/jas-d-13-0240.1.

- Bogenschutz, P. A., A. Gettelman, C. Hannay, V. E. Larson, R. B. Neale, C. Craig,
- and C.-C. Chen (2018), The path to CAM6: Coupled simulations with CAM5.4
- and CAM5.5, Geosci. Model Dev., 11(1), 235–255, doi:10.5194/gmd-11-235-2018.
- Bony, S., and K. A. Emanuel (2005), On the role of moist processes in tropical in-
- traseasonal variability: Cloud-radiation and moisture-convection feedbacks, J.
- Atmos. Sci., 62(8), 2770–2789, doi:10.1175/jas3506.1.
- Bretherton, C. S. (2015), Insights into low-latitude cloud feedbacks from high-
- resolution models, Philosophical Transactions of the Royal Society of London
- A: Mathematical, Physical and Engineering Sciences, 373 (2054).
- Bretherton, C. S., and A. H. Sobel (2002), A simple model of a convectively coupled
- Walker circulation using the weak temperature gradient approximation, J. Cli-
- $mate, 15(20), 2907-2920, doi:10.1175/1520-0442(2002)015\langle 2907:asmoac \rangle 2.0.co; 2.0.c$
- Bretherton, C. S., M. E. Peters, and L. E. Back (2004), Relationships between water
- vapor path and precipitation over the tropical oceans, J. Climate, 17(7), 1517–
- 1528, doi:10.1175/1520-0442(2004)017(1517:rbwvpa)2.0.co;2.
- ⁴³⁵ Ceppi, P., and D. L. Hartmann (2016), Clouds and the atmospheric circulation
- response to warming, J. Climate, 29(2), 783–799, doi:10.1175/jcli-d-15-0394.1.
- 437 Computational and Information Systems Laboratory (2017), Cheyenne: HPE/SGI
- ICE XA System (University Community Computing). Boulder, CO: National
- Center for Atmospheric Research, doi:10.5065/D6RX99HX.
- 440 Crueger, T., and B. Stevens (2015), The effect of atmospheric radiative heating by
- clouds on the madden-julian oscillation, J. Adv. Model. Earth Syst., 7(2), 854-
- 864, doi:10.1002/2015ms000434.
- Duchon, C. E. (1979), Lanczos filtering in one and two dimensions, J. Appl. Meteor.,
- 18(8), 1016-1022, doi:10.1175/1520-0450(1979)018(1016:lfioat)2.0.co;2.
- Emanuel, K. (2019), Inferences from simple models of slow, convectively coupled
- processes, J. Atmos. Sci., 76(1), 195-208, doi:10.1175/jas-d-18-0090.1.
- Fermepin, S., and S. Bony (2014), Influence of low-cloud radiative effects on trop-
- ical circulation and precipitation, J. Adv. Model. Earth Syst., 6(3), 513–526,
- doi:10.1002/2013ms000288.
- Firestone, J. K., and B. A. Albrecht (1986), The structure of the atmospheric
- boundary layer in the central equatorial pacific during january and february
- of FGGE, Mon. Wea. Rev., 114(11), 2219–2232, doi:10.1175/1520-0493(1986)

- 453 $114\langle 2219:tsotab\rangle 2.0.co; 2.$
- Fuchs, Z., and D. J. Raymond (2002), Large-scale modes of a nonrotating atmo-
- sphere with water vapor and cloud-radiation feedbacks, J. Atmos. Sci., 59(10),
- 1669-1679, doi:10.1175/1520-0469(2002)059(1669:lsmoan)2.0.co;2.
- Fuchs, Z., and D. J. Raymond (2005), Large-scale modes in a rotating atmosphere
- with radiative-convective instability and WISHE, J. Atmos. Sci., 62(11), 4084-
- 4094, doi:10.1175/jas3582.1.
- 460 Grabowski, W. W. (2003), MJO-like coherent structures: Sensitivity simulations
- using the cloud-resolving convection parameterization (CRCP), J. Atmos. Sci.,
- 60(6), 847-864, doi:10.1175/1520-0469(2003)060(0847:mlcsss)2.0.co;2.
- Grabowski, W. W., and M. W. Moncrieff (2001), Large-scale organization of tropi-
- cal convection in two-dimensional explicit numerical simulations, Quart. J. Roy.
- Meteor. Soc., 127(572), 445-468, doi:10.1002/qj.49712757211.
- Grise, K. M., B. Medeiros, J. J. Benedict, and J. G. Olson (2019), Investigating the
- influence of cloud radiative effects on the extratropical storm tracks, Geophys.
- 468 Res. Lett., 46(13), 7700-7707, doi:10.1029/2019gl083542.
- 469 Haertel, P. T., G. N. Kiladis, A. Denno, and T. M. Rickenbach (2008), Vertical-
- mode decompositions of 2-day waves and the madden–julian oscillation, J. Atmos.
- Sci., 65(3), 813-833, doi:10.1175/2007 jas 2314.1.
- Hannah, W. M., and E. D. Maloney (2014), The moist static energy budget in
- NCAR CAM5 hindcasts during DYNAMO, J. Adv. Model. Earth Syst., 6(2),
- 420-440, doi:10.1002/2013ms000272.
- Harrop, B. E., and D. L. Hartmann (2016), The role of cloud radiative heating
- in determining the location of the ITCZ in aquaplanet simulations, J. Climate,
- 29(8), 2741–2763, doi:10.1175/jcli-d-15-0521.1.
- Hartmann, D. L., and D. A. Short (1980), On the use of earth radiation budget
- statistics for studies of clouds and climate, J. Atmos. Sci., 37(6), 1233–1250,
- doi: $10.1175/1520-0469(1980)037\langle 1233:otuoer \rangle 2.0.co; 2.$
- Hu, Q., and D. A. Randall (1994), Low-frequency oscillations in radiative-convective
- systems, J. Atmos. Sci., 51(8), 1089-1099, doi:10.1175/1520-0469(1994)051(1089):
- lfoirc $\rangle 2.0.$ co;2.
- Huffman, G. J., D. T. Bolvin, E. J. Nelkin, D. B. Wolff, R. F. Adler, G. Gu,
- Y. Hong, K. P. Bowman, and E. F. Stocker (2007), The TRMM multisatellite pre-

- cipitation analysis (TMPA): Quasi-global, multiyear, combined-sensor precipita-
- tion estimates at fine scales, J. Hydrometeor., 8(1), 38-55, doi:10.1175/jhm560.1.
- Hung, M.-P., J.-L. Lin, W. Wang, D. Kim, T. Shinoda, and S. J. Weaver (2013),
- MJO and convectively coupled equatorial waves simulated by CMIP5 climate
- models, J. Climate, 26(17), 6185–6214, doi:10.1175/jcli-d-12-00541.1.
- Khairoutdinov, M. F., and K. Emanuel (2018), Intraseasonal variability in a cloud-
- permitting near-global equatorial aquaplanet model, J. Atmos. Sci., 75 (12), 4337-
- 4355, doi:10.1175/jas-d-18-0152.1.
- Kim, D., A. H. Sobel, and I.-S. Kang (2011a), A mechanism denial study
- on the Madden-Julian Oscillation, J. Adv. Model. Earth Syst., 3(4), doi:
- 496 10.1029/2011ms000081.
- 497 Kim, D., A. H. Sobel, E. D. Maloney, D. M. W. Frierson, and I.-S. Kang (2011b), A
- systematic relationship between intraseasonal variability and mean state bias in
- agem simulations, J. Climate, 24(21), 5506-5520, doi:10.1175/2011jcli4177.1.
- Kim, D., M.-S. Ahn, I.-S. Kang, and A. D. D. Genio (2015), Role of longwave
- cloud-radiation feedback in the simulation of the madden-julian oscillation, J.
- Climate, 28(17), 6979-6994, doi:10.1175/jcli-d-14-00767.1.
- Langen, P. L., R. G. Graversen, and T. Mauritsen (2012), Separation of contribu-
- tions from radiative feedbacks to polar amplification on an aquaplanet, J. Climate,
- 505 25(8), 3010–3024, doi:10.1175/jcli-d-11-00246.1.
- Lee, M.-I., I.-S. Kang, J.-K. Kim, and B. E. Mapes (2001), Influence of cloud-
- radiation interaction on simulating tropical intraseasonal oscillation with an
- atmospheric general circulation model, J. Geophys. Res.: Atmos., 106(D13),
- ⁵⁰⁹ 14,219–14,233, doi:10.1029/2001jd900143.
- Lin, J.-L., and B. E. Mapes (2004), Radiation budget of the tropical intraseasonal
- oscillation, J. Atmos. Sci., 61(16), 2050–2062, doi:10.1175/1520-0469(2004)
- $061\langle 2050:rbotti \rangle 2.0.co; 2.$
- Lin, J.-L., D. Kim, M.-I. Lee, and I.-S. Kang (2007), Effects of cloud-radiative heat-
- ing on atmospheric general circulation model (AGCM) simulations of convectively
- coupled equatorial waves, J. Geophys. Res., 112(D24), doi:10.1029/2006jd008291.
- Ma, D., and Z. Kuang (2016), A mechanism-denial study on the Madden-Julian Os-
- cillation with reduced interference from mean state changes, Geophys. Res. Lett.,
- 43(6), 2989-2997, doi:10.1002/2016gl067702.

- Madden, R. A., and P. R. Julian (1971), Detection of a 40–50 day oscillation
- in the zonal wind in the tropical pacific, J. Atmos. Sci., 28(5), 702–708, doi:
- 10.1175/1520-0469(1971)028(0702:doadoi)2.0.co;2.
- Maloney, E. D. (2009), The moist static energy budget of a composite tropical in-
- traseasonal oscillation in a climate model, J. Climate, 22(3), 711–729.
- Mapes, B. E. (2000), Convective inhibition, subgrid-scale triggering energy, and
- stratiform instability in a toy tropical wave model, J. Atmos. Sci., 57(10), 1515–
- 1535, doi:10.1175/1520-0469(2000)057 $\langle 1515$:cisste $\rangle 2.0.$ co;2.
- Matthews, A. J. (2000), Propagation mechanisms for the madden-julian oscillation,
- See Quart. J. Roy. Meteor. Soc., 126 (569), 2637–2651, doi:10.1002/qj.49712656902.
- Mauritsen, T., R. G. Graversen, D. Klocke, P. L. Langen, B. Stevens, and
- L. Tomassini (2013), Climate feedback efficiency and synergy, Clim. Dyn., 41 (9-
- 10), 2539–2554, doi:10.1007/s00382-013-1808-7.
- Middlemas, E. A., A. C. Clement, B. Medeiros, and B. Kirtman (2019), Cloud radia-
- tive feedbacks and El Niño-Southern Oscillation, J. Climate, 32(15), 4661-4680,
- doi:10.1175/jcli-d-18-0842.1.
- Neelin, J. D., and I. M. Held (1987), Modeling tropical convergence based on
- the moist static energy budget, Mon. Wea. Rev., 115(1), 3–12, doi:10.1175/
- $1520-0493(1987)115\langle 0003:mtcbot \rangle 2.0.co; 2.$
- Paternoster, R., R. Brame, P. Mazerolle, and A. Piquero (1998), Using the correct
- statistical test for the equality of regression coefficients, Criminology, 36(4), 859-
- 540 866, doi:10.1111/j.1745-9125.1998.tb01268.x.
- Pritchard, M. S., and C. S. Bretherton (2014), Causal Evidence that Rotational
- Moisture Advection is Critical to the Superparameterized Madden–Julian Oscilla-
- tion, J. Atmos. Sci., 71(2), 800–815, doi:10.1175/JAS-D-13-0119.1.
- Rädel, G., T. Mauritsen, B. Stevens, D. Dommenget, D. Matei, K. Bellomo, and
- A. Clement (2016), Amplification of El Niño by cloud longwave coupling to atmo-
- spheric circulation, *Nature Geosci.*, 9(2), 106–110, doi:10.1038/ngeo2630.
- Randall, D., M. Khairoutdinov, A. Arakawa, and W. Grabowski (2003), Breaking
- the cloud parameterization deadlock, Bull. Amer. Meteor. Soc., 84(11), 1547–
- 549 1564, doi:10.1175/bams-84-11-1547.
- Raymond, D. J. (1995), Regulation of moist convection over the west pacific warm
- pool, J. Atmos. Sci., 52(22), 3945-3959, doi:10.1175/1520-0469(1995)052(3945:

- romcot \rangle 2.0.co;2.
- Raymond, D. J. (2000), The Hadley circulation as a radiative-convective insta-
- bility, J. Atmos. Sci., 57(9), 1286-1297, doi:10.1175/1520-0469(2000)057(1286:
- thcaar2.0.co;2.
- Raymond, D. J. (2001), A new model of the Madden–Julian Oscillation, J. Atmos.
- $Sci., 58(18), 2807-2819, doi:10.1175/1520-0469(2001)058\langle 2807: anmotm \rangle 2.0.co; 2.0.$
- Raymond, D. J., and Ž. Fuchs (2007), Convectively coupled gravity and mois-
- ture modes in a simple atmospheric model, $Tellus\ A,\ 59(5),\ 627-640,\ doi:$
- 10.1111/j.1600-0870.2007.00268.x.
- Raymond, D. J., and Ž. Fuchs (2009), Moisture modes and the Madden–Julian
- Oscillation, J. Climate, 22(11), 3031–3046, doi:10.1175/2008jcli2739.1.
- Raymond, D. J., S. L. Sessions, A. H. Sobel, and Ž. Fuchs (2009), The mechanics of
- gross moist stability, J. Adv. Model. Earth Syst., 1(3), doi:10.3894/JAMES.2009.1.
- 565 9.
- Roundy, P. E. (2012), Tropical-extratropical Interactions, chap. 14, pp. 497–512,
- Springer, Berlin, Heidelberg.
- Schäfer, S. A. K., and A. Voigt (2018), Radiation weakens idealized midlatitude
- cyclones, Geophys. Res. Lett., 45(6), 2833–2841, doi:10.1002/2017gl076726.
- 570 Shi, X., D. Kim, Á. F. Adames, and J. Sukhatme (2018), WISHE-moisture mode
- in an aquaplanet simulation, J. Adv. Model. Earth Syst., 10(10), 2393–2407, doi:
- 572 10.1029/2018ms001441.
- 573 Slingo, A., and J. M. Slingo (1988), The response of a general circulation model to
- cloud longwave radiative forcing. I: Introduction and initial experiments, Quart. J.
- 875 Roy. Meteor. Soc., 114 (482), 1027–1062, doi:10.1002/qj.49711448209.
- Sobel, A., and E. Maloney (2013), Moisture modes and the eastward propagation of
- the MJO, J. Atmos. Sci., 70(1), 187–192, doi:10.1175/jas-d-12-0189.1.
- Sobel, A. H., and H. Gildor (2003), A simple time-dependent model of SST hot
- spots, J. Climate, 16(23), 3978-3992, doi:10.1175/1520-0442(2003)016(3978:
- astmos $\rangle 2.0.co; 2.$
- Sobel, A. H., J. Nilsson, and L. M. Polvani (2001), The weak temperature gradi-
- ent approximation and balanced tropical moisture waves, J. Atmos. Sci., 58(23),
- 3650-3665, doi:10.1175/1520-0469(2001)058(3650:twtgaa)2.0.co;2.

- Sugiyama, M. (2009), The moisture mode in the Quasi-Equilibrium Tropical Circula-
- tion Model. Part I: Analysis based on the weak temperature gradient approxima-
- tion, J. Atmos. Sci., 66(6), 1507-1523, doi:10.1175/2008jas2690.1.
- Wheeler, M., and G. N. Kiladis (1999), Convectively coupled equatorial waves:
- Analysis of clouds and temperature in the wavenumber–frequency domain, J. At-
- $mos. Sci., 56(3), 374-399, doi:10.1175/1520-0469(1999)056\langle 0374:CCEWAO\rangle 2.0.$
- 590 CO;2.
- ⁵⁹¹ Zhang, C. (2005), Madden-Julian Oscillation, Rev. Geophys., 43(2), doi:10.1029/
- ⁵⁹² 2004rg000158.

Table 1. Zero-lag regression coefficients for selected anomaly fields and disturbances, scaled by precipitation intensity a

Type	Variable	Unit	FCTL	FLOCK	FLOCK-FCTL
MJO	PW	$\mathrm{mm}/(\mathrm{mm}\mathrm{d}^{-1})$	0.66	0.53	-0.13*
	LH	${ m Wm^{-2}/(mmd^{-1})}$	1.34	2.88	+1.54*
	DCIN	$\rm Jkg^{-1}/(mmd^{-1})$	-226	-250	-24.9
	$\overline{h^*}_{\mathrm{t}}$	$\rm Jkg^{-1}/(mmd^{-1})$	-103	-139	-36.4
	$\overline{h}_{\mathrm{PBL}}$	$\rm Jkg^{-1}/(mmd^{-1})$	123	111	-11.6
Kelvin	PW	$\mathrm{mm}/(\mathrm{mm}\mathrm{d}^{-1})$	0.38	0.44	+0.14
	LH	${ m Wm^{-2}/(mmd^{-1})}$	-0.50	-0.29	+0.21
	DCIN	$\rm Jkg^{-1}/(mmd^{-1})$	-116	-205	-89.2*
	$\overline{h^*}_{\mathrm{t}}$	$\rm Jkg^{-1}/(mmd^{-1})$	-140	-206	-65.6*
	$\overline{h}_{\mathrm{PBL}}$	$\rm Jkg^{-1}/(mmd^{-1})$	-24.2	-0.62	+23.6

^aZero-lag regression coefficients of unfiltered anomaly fields based on (top) equatorial MJO-filtered precipitation at 155°E and (bottom) Kelvin wave-filtered precipitation at 105°E for FCTL, FLOCK, and the FLOCK–FCTL difference. Variables shown are scaled to 1 mm d⁻¹ of the index and are precipitable water (PW), surface latent heat flux (LH), deep convective inhibition (DCIN = $\overline{h^*}_{\rm t}$ – $\overline{h}_{\rm PBL}$), and mass-weighted vertical averages of saturated MSE from 700–800 hPa ($\overline{h^*}_{\rm t}$) and MSE from 800 hPa–surface ($\overline{h}_{\rm PBL}$). Differences greater than the 95% statistical significance level are emboldened and starred. See Text S3 for methods.

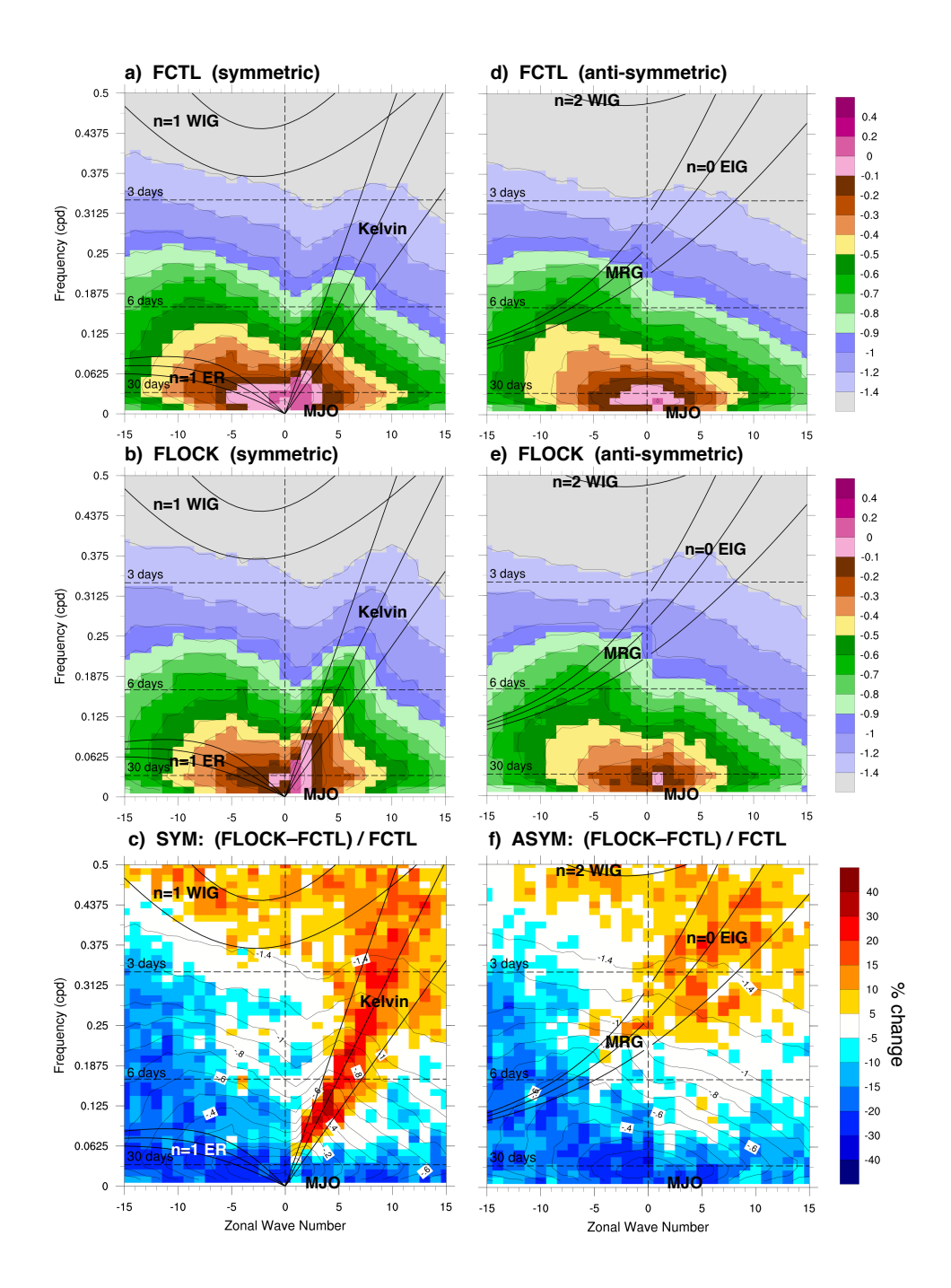


Figure 1. Precipitation zonal wavenumber-frequency power spectra for (a) the component symmetric about the equator for FCTL, (b) the FLOCK symmetric component, and (c) (FLOCK–FCTL)/FCTL expressed in percent. Powers are summed over 15°S–15°N and shown using log base-10 scaling. Thick black lines indicate shallow water dispersion curves for equivalent depths of 12, 25, and 50 m. Westward and eastward inertia-gravity waves are WIG and EIG; other wave types are discussed in text. Meridional mode number n follows conventional shallow water theory. (d–f) As in (a–c) but for the anti-symmetric component. In (c) and (f), power contours are redrawn from (a) and (c).

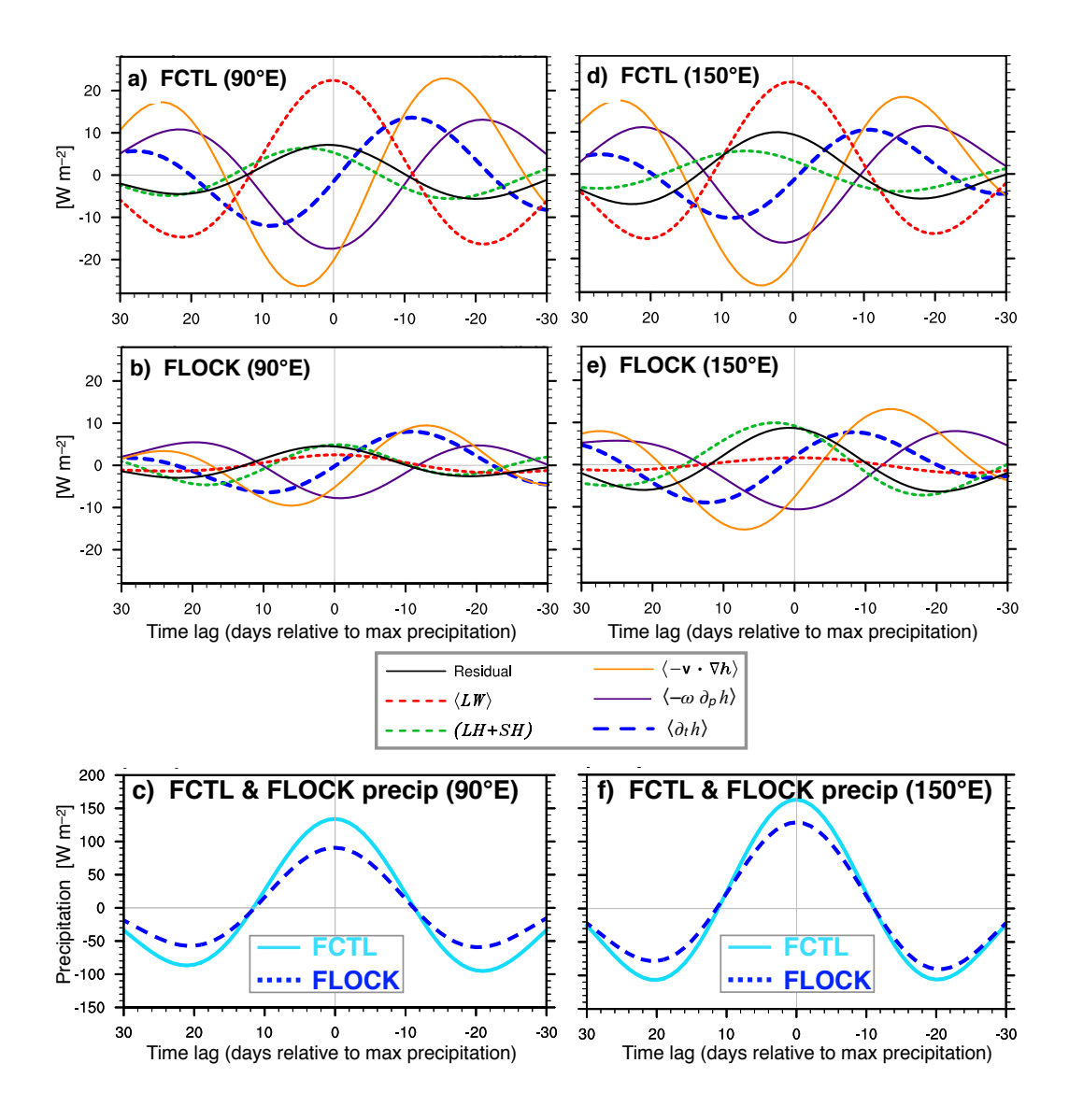


Figure 2. Latitudinally averaged (10°S-5°N) and bandpass-filtered (30–100-day) anomaly terms of the column MSE budget for (top) FCTL and (middle) FLOCK lag composited based on identically filtered precipitation at 90°E (left) and 150°E (right). (c,e) Corresponding FCTL and FLOCK precipitation anomalies. The budget residual is shown as a black line. See Text S1 for budget equation and method details.

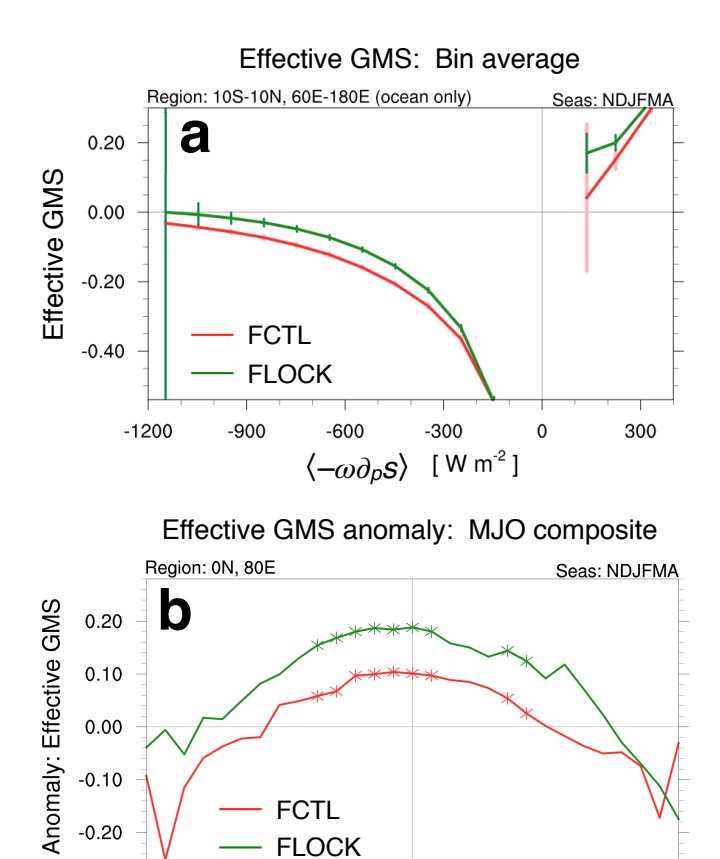


Figure 3. (a) Effective GMS based on bin averages of column dry static energy advection $\langle -\omega \partial_p s \rangle$ for FCTL and FLOCK. Vertical bars indicate 95% confidence limits. Bins within $150\,\mathrm{W\,m^{-2}}$ of zero are masked due to increased volatility of the GMS quotient. All data are restricted to ocean points within the region $(10^\circ\mathrm{S}-10^\circ\mathrm{N}, 60^\circ\mathrm{E}-180^\circ\mathrm{E})$ and the November-April season. (b) Effective GMS anomalies lag composited based on identified MJO events. Starred points indicate FLOCK–FCTL differences exceeding the 90% statistical significance level. See Text S4 and S5 for method details.

Lag [days since max precip]

-5

-10